ISSN 1064-2269, Journal of Communications Technology and Electronics, 2022, Vol. 67, No. 7, pp. 911–917. © Pleiades Publishing, Inc., 2022.
Russian Text © The Author(s), 2022, published in Radiotekhnika i Elektronika, 2022, Vol. 67, No. 7, pp. 715–721.

PHYSICAL PROCESSES IN ELECTRON DEVICES

ZnSe and ZnCdSe/ZnSe Photodetectors for Visible Spectral Range: Comparative Parameters

S. V. Averin[a], *, L. Yu. Zakharov[a], V. A. Zhitov[a], and V. M. Kotov[a]

[a] *Kotelnikov Institute of Radioengineering and Electronics (Fryazino Branch), Russian Academy of Sciences, Fryazino, Moscow oblast, 141190 Russia*

**e-mail: sva278@ire216.msk.su*

Received December 16, 2021; revised December 16, 2021; accepted January 19, 2022

Abstract—The spectral response and quantum efficiency of the visible-range photodetectors based on ZnSe and ZnCdSe/ZnSe heterostructures are experimentally studied. The spectral response of the detectors is characterized under various bias conditions. A model of a decrease in the effective height of a reverse-biased Schottky contact under irradiation is used to interpret the internal amplification of the detectors.

DOI: 10.1134/S106422692207004X

INTRODUCTION

Until recently, the detection of UV and visible radiation was performed almost exclusively with the aid of Si and GaAs detectors [1]. The main disadvantage of such detectors is the degradation of parameters under irradiation at a photon energy that is much greater than the band gap of Si and GaAs. In addition, Si and GaAs photodetectors exhibit the maximum sensitivity in the IR range, so that a correction using an appropriate filter is needed for operation in the blue and violet parts of the spectrum, which leads to a complication of the receiving system and a decrease in its sensitivity [1–3]. For these reasons, wide bandgap semiconductor materials (GaN, ZnO, ZnSe and their solid solutions) are being intensively studied as active layers of UV and visible photodetectors [1, 4]. A wide-bandgap semiconductor provides a low dark current and high reliability under irradiation with high-energy photons, and a narrow-band response of the detector can be implemented using selection of the parameters of the heteroepitaxial layers. Such an approach provides filtering of the received desired signal and, thereby, an increase in the noise immunity of the optical information system [4]. It is also known that wide-bandgap semiconductor materials have a significantly higher thermal conductivity and radiation resistance in comparison with Si and GaAs. Thus, the corresponding devices can be used at much higher temperatures and powers of received radiation whereas the strength of chemical bonds in wide-bandgap semiconductors ensures an increased radiation resistance [1].

In many works, various types of photodetectors based on wide-bandgap semiconductor materials and heterostructures have been fabricated and studied, in particular, *p*–*n*-junction detectors [5], *p*–*i*–*n* photodiodes [6, 7], Schottky barrier photodiodes [8], and photodetectors in a contact system metal–semiconductor–metal (MSM) [9, 10]. Particular attention was paid to narrow-band detectors. A narrowband response with a FWHM of 14 nm has been obtained for the AlGaN/GaN MSM diodes at a wavelength of 361 nm [11]. An even narrower response with FWHM = 7 nm at a wavelength of about 370 nm has been obtained for the MSM detectors based on the (Mg,Zn)O heterostructure [12]. The detecting properties of the MSM diodes based on low-dimensional heterostructures with the ZnCdS quantum wells separated by ZnMgS and ZnS barrier layers have been studied in [13]. The detectors provide two-color detection of optical signals at wavelengths of 350 and 450 nm with FWHMs of 18 and 50 nm, respectively. It is seen that there has been considerable recent interest in narrow-band photodetectors of the visible and UV spectral ranges based on wide-bandgap semiconductor materials.

In this work, we study the characteristics of the spectral response and quantum efficiency of the visible-range MSM detectors. For comparison, two types of MSM photodetectors were fabricated: ZnSe detectors and detectors based on the ZnCdSe/ZnSe heterobarrier structure. The ZnSe MSM detector makes it possible to obtain a broadband response in a wavelength interval of 330–465 nm with a maximum responsivity of 0.14 A/W at a wavelength of 460 nm, which corresponds to a detector quantum efficiency of 38%. The MSM detector based on the ZnCdSe/ZnSe heterojunction provides an effective narrow-band response with FWHM = 4.3 nm, a responsivity of 2.27 A/W, and a quantum efficiency of 612% at a wavelength of 460 nm.

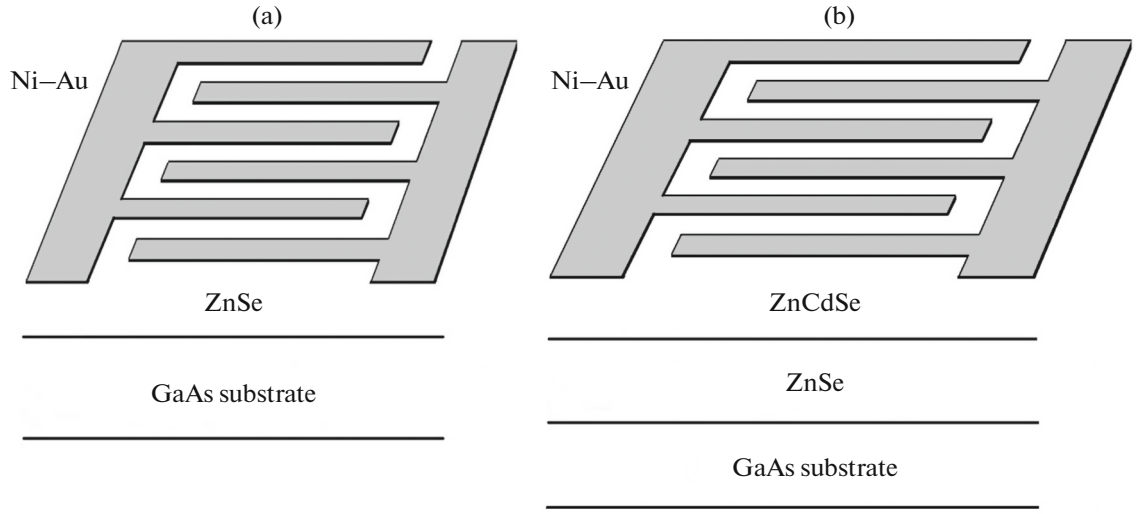

Fig. 1. Epitaxial layers and interdigitated contacts of (a) D1 and (b) D2 MSM diodes.

1. EXPERIMENTAL RESULTS

Zinc selenide and solid solutions based on this substance (ZnSSe, ZnSTe, and ZnMgBeSe) are promising semiconductor materials for optoelectronic devices working in the visible and UV spectral ranges [1]. They can be grown lattice-matched with a GaAs substrate, which provides the integration of the photodetector with amplification and signal processing circuits based on GaAs electronics. Fabrication of *p*–*n*- and *p*–*i*–*n*-photodiodes based on ZnSe and ZnSSe meets difficulties related to the formation of a high-quality ohmic contact to the *p*-region of the detector [14]. Production of heavily doped *p*-type ZnSe and ZnSSe is still a problem that impedes fabrication of optoelectronic devices based on such wide-bandgap materials. For this reason, a planar surface-barrier diode structure based on double rectifying contacts in the MSM system was chosen as the basic structure of photodiodes in this work [15, 16]. In such a detector, we can use a semiconductor material of only one type of conductivity in the absence of ohmic contacts. The area of the active region of the MSM diode is four times greater than the area of the *p*–*i*–*n*-diode at equal capacitances. This circumstance substantially facilitates focusing of the received optical radiation onto the light-sensitive region of the detector. In addition, due to the location of the depletion region of the reverse-biased Schottky contact directly under the surface of the semiconductor structure, such a detector design is preferred in the UV and visible spectral ranges in comparison with the *p*–*i*–*n* diode and the *p*–*n*-junction detector, in which light passes through the *p*-junction region of the diode, where a significant part of it is lost.

Two types of MSM detectors (D1 and D2) were investigated. Photodiode D1 is fabricated as interdigitated Schottky barrier contacts to a 550-nm-thick ZnSe epitaxial film grown with the aid of metalorganic vapor-phase epitaxy (MOVPE) on a 300-nm-thick semi-insulating GaAs substrate (Fig. 1a). For the fabrication of the Schottky barrier contacts of the MPM diode, two layers were sputtered: barrier Ni (90 nm) and protective Au (70 nm). Then, the interdigitated contacts of the MSM diode with a width of 2.8 μm, a length of 100 μm, and a distance of 3 μm between them were formed on the surface of the structure with the aid of photolithography. The photosensitive area of the MSM detector is 100 × 100 μm^2.

Photodiode D2 was fabricated in a similar way with the same configuration of interdigitated contacts, but the ZnCdSe/ZnSe heterobarrier structure was used as the active layer of the detector. The thicknesses of the ZnCdSe and ZnSe layers (132 and 805 nm, respectively) were calculated using the reflection spectra. The details of the deposition of epitaxial films can be found in [17].

The surface morphology of the grown epitaxial films of the D1 and D2 diodes was studied using an AIST-NT Smart SPM atomic force microscope. The surface of the semiconductor structures of the D1 and D2 diodes was quite dense and consisted of uniformly distributed single-crystal units. The experimental rms roughness of the growth surface of the semiconductor structure of the D2 diode over an area of 20 × 20 μm^2 was RMS = 22 nm. Figure 2 shows a microphotograph of a surface fragment of the MSM photodiode (D2).

1.1. Characteristics of the MSM Diodes

The *I*–*V* characteristics of the MSM diodes were studied at room temperature using an analyzer of the parameters of semiconductor devices. Figure 3 shows the characteristics at different polarities of bias voltage. The dark current of the D2 diode is slightly lower

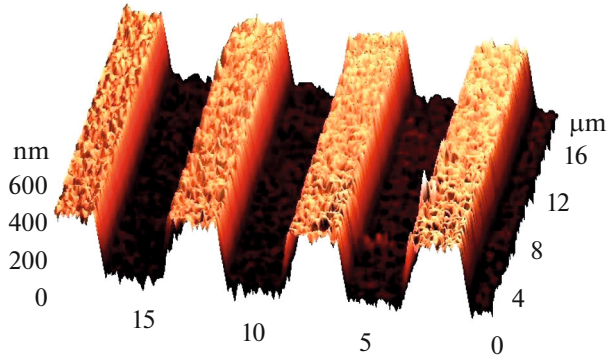

Fig. 2. Microphotograph of a surface fragment of the D2 MSM photodetector (the length of the Ni–Au interdigitated contacts is 100 μm, the width is 2.8 μm, and the distance between the contacts is 3 μm).

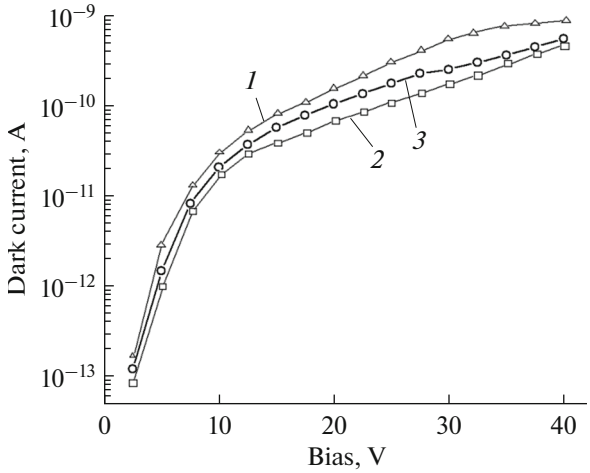

Fig. 3. Dark currents of (*1*) D1 diode and (*2*) forward- and (*3*) reverse-biased D2 diode.

due to the ZnCdSe surface layer. At a bias voltage of 30 V, the dark current of this diode is 2×10^{-10} A, which is comparable with the dark current of an MSM diode based on a low-dimensional ZnCdS/ZnMgS/GaP heterostructure [18]. The dark current of the D1 homoepitaxial ZnSe photodetectors at the same bias is 5×10^{-10} A. Since both shot noise and $1/f$ noise are proportional to the current flowing through the junction, a low dark current improves the signal-to-noise ratio of the detection system. The dark current in the diode structure depends on the height of the barrier contact. The MSM diode consists of two series-connected Schottky barrier contacts. When voltage is applied to the diode, one contact is forward-biased and the second contact is reverse-biased. Thus, despite the fact that the polarity of the bias voltage across the diode can be reversed, only the reverse branches of the I–V characteristics can be measured for each contact.

Therefore, we cannot study the MSM structures using the conventional method for estimation of the parameters of the Schottky barrier based on measurement of the forward branch of its I–V characteristic [19, 20]. We measured the height of the Schottky barrier in the MSM system of contacts of the D1 and D2 diodes with the aid of the method of [21]. The analysis shows that the dark current of the barrier contacts under study is well described in terms of the theory of thermionic emission. The experimental and calculated heights of the potential Schottky barrier in the D1 and D2 diodes are 1.15 and 1.3 eV, respectively, and the ideality factor of junction in both cases is $n \sim 1.2$. Such parameters indicate the absence of a sufficiently thick intermediate oxide layer in the metal–semiconductor contacts under study and a relatively high quality of the Schottky barriers in the fabricated MSM diodes. The experimental height of the potential barrier of the Ni/Au–ZnSe contact is close to the previously published results (1.17 eV [22] and 1.20 eV [23] for the Au–ZnSe contact).

Note also a slight asymmetry of the I–V characteristics of the MSM diode D2 for forward and reverse biases due to minor differences in the heights of the potential barriers of two series-connected Schottky interdigitated barrier contacts. Presumably, this is due to different densities of states at the metal–semiconductor interface of two adjacent barrier contacts and inevitable growth defects, leading to inhomogeneity of the surface of the grown semiconductor structure and, hence, unequal effective areas of two neighboring contacts. For the D1 diode, we do not observe differences of the I–V characteristics for forward and reverse biases. The breakdown voltages of the D1 and D2 detectors range from 90 to 100 V, which indicates potential resistance to possible bias voltage surges under real conditions. In addition, high breakdown voltages and, consequently, high electric fields in such semiconductor structures make it possible to use them in MSM diodes with submicron intercontact gaps to increase the photodetector bandwidth due to an increase in the drift velocity of photogenerated carriers at high fields [24].

1.2. Spectral Responsivity of the Detectors

The spectral responsivity of the diode structures under study was measured at room temperature using a xenon lamp as a radiation source. The radiation of the lamp having passed through a monochromator was chopped at a frequency of 400 Hz and focused on the active area of the MPM diode by a system of optical lenses. The resulting photocurrent was measured with a PAR-124A lock-in amplifier. The power of optical radiation incident on the photodiode was measured with a calibrated silicon photodiode. The responsivity of the photodetector was calculated as the ratio of the measured signal current of the MSM diode to the radi-

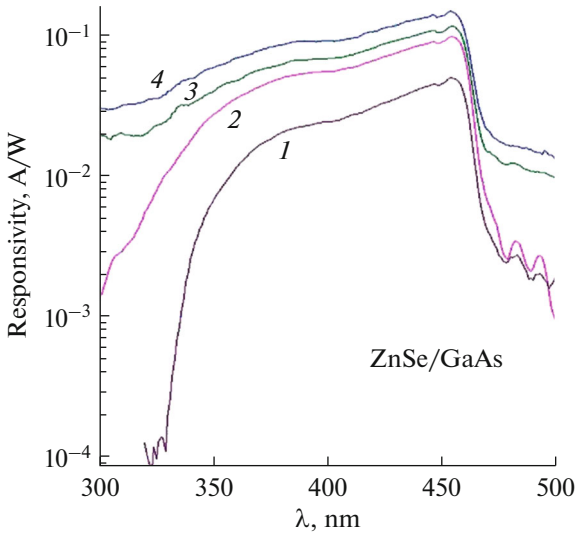

Fig. 4. Plot of the responsivity of the D1 MSM photodetector vs. wavelength for bias voltages of (*1*) 5, (*2*) 15, (*3*) 20, and (*4*) 30 V.

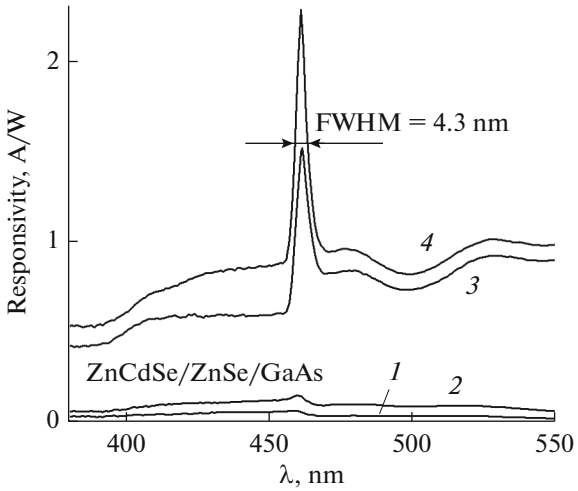

Fig. 5. Spectra of the responsivity of the D2 MSM detector at bias voltages of (*1*) 5, (*2*) 10, (*3*) 20, and (*4*) 30 V.

ation power of the xenon lamp incident on the diode at the corresponding wavelength.

Figure 4 presents the dependence of the responsivity of the D1 detector on the bias voltage. The detector provides a broadband response in a wavelength interval of 330–465 nm. The detector response signal sharply increases with an increase in the bias in an interval of 5–15 V, which is a consequence of the expansion of the depletion region between the interdigitated contacts of the diode. The maximum of the detector response signal is at a wavelength of 460 nm, which corresponds to a ZnSe band gap of 2.7 eV. One of the practical applications of the D1 detector can be its use for detection of the UV radiation that is harmful to humans. It is well known that an excess dose of solar radiation can lead to diseases [4]. The photosensitivity interval of the D1 detector coincides with the interval of the maximum effect of the pigmentation solar radiation (0.36–0.44 μm), so that the photodetector based on the D1 MSM diode can serve as a tan sensor.

Figure 5 shows the dependence of the photoresponse of the MSM detector D2 based on the ZnCdSe/ZnSe/GaAs heterostructure on the wavelength of optical radiation. Such a detector provides a fairly narrow-band response. At a wavelength of 460 nm, the FWHM of the detector response is 4.3 nm. The results of [1, 25] show that the ZnSe, ZnSSe photodetectors based on the Schottky barrier provide a sharp drop in photosensitivity in the long-wavelength part of the response signal (the long-wavelength cutoff). Figure 5 also shows such a result. When optical signals are detected at shorter wavelengths, an increase in the photon energy leads to a sharp increase in the absorption coefficient of radiation incident on the detector. The radiation is absorbed closer and closer to the surface of the heterostructure [19, 26]. In this case, the concentration of photogenerated electrons and holes in the narrow surface region of ZnCdSe is very high, which causes a sharp increase in the probability of surface and bulk recombination and a decrease in the lifetime of carriers [27–29]. The carriers recombine in the thin ZnCdSe layer before they reach the interdigitated contacts of the MSM diode.

Figure 6 presents the dependence of the response signal of the MSM diodes D1 and D2 on the bias voltage. The response of the detector to the optical signal, first, increases linearly with increasing bias and, then, a region of photocurrent saturation appears. 2D simulation of an MSM diode shows that the detector operates under conditions for partial depletion of the active interelectrode region of the diode when the gap between the interdigitated contacts is 3 μm and the bias voltage is less than 10 V [30]. Such a result is proven by the low level of the detector response signal at bias voltages ranging from 5 to 10 V (Fig. 6). An increase in the bias voltage leads to the expansion of the depletion region of the reverse-biased Schottky contact, and the maximum responsivity of the D2 detector at a wavelength of 460 nm rapidly increases from 0.05 A/W at 5 V to 1.5 A/W at 20 V (Fig. 6). This leads to an increase in the quantum efficiency of the photodetector from 13.5% to 400%. The voltage that determines the beginning of the saturation of the detector photocurrent (the condition for flat bands of metal–semiconductor contact) is calculated using the equation [31]

$$V = \frac{qN_d t^2}{2\epsilon_s},$$

where N_d is the concentration of free carriers in the surface layer of semiconductor, ε_s is the permittivity, and t is the intercontact gap.

The level of doping for the surface layer of the ZnCdSe/ZnSe heterostructure of the D2 diode was determined from the capacitance–voltage characteristic of the Schottky contact: $N_d = 2 \times 10^{15}$ cm^{-3}. For $t = 3$ μm, we obtain $V = 20$ V, which is in good agreement with our experiment. The experimental results show that the concentration of free carriers in the surface layer of the semiconductor structure of the D1 diode is 10^{15} cm^{-3}. Thus, the bias voltage corresponding to the condition for flat bands for the D1 diode decreases to ~10 V (Fig. 6).

At a bias voltage of 30 V, the measured responsivity of the MSM diode D1 is 0.14 A/W and the calculated quantum efficiency is 38%, which is in good agreement with the results of [22, 32, 33]. The responsivity of the D2 detector at the same wavelength is 2.27 A/W, and the quantum efficiency is 612%. Thus, at the same bias voltage, the responsivity of the D2 heterobarrier MSM diode is about 16 times higher than the responsivity of the D1 homoepitaxial diode. The quantum efficiency of the D2 detector is much higher than 100%, which indicates an internal amplification of the photocurrent in such a diode structure. Several theories have been proposed to interpret amplification of photocurrent in MSM detectors based on the Schottky barrier; in particular, one of them assumes enhancement of electron tunneling through the barrier [19, 34]. However, the ideality factor of the barrier contact in our structure is close to unity, which indicates the key role of the above-barrier electron emission in the current conduction in the diode. We assume that the photoamplification observed in the D2 detector under study is due to trapping of minority carriers (holes) at the trapping centers of the ZnCdSe/ZnSe heterojunction. The existence of trapping centers at the interface between two semiconductors is well known from [12, 35]. Under irradiation of the junction, the holes photogenerated in the depletion region of the reverse-biased contact are trapped at the trapping centers of the ZnCdSe/ZnSe heterojunction and produce a positive charge $Q_{hi} = qN_{hi}$, where N_{hi} is the concentration of trapping centers at the heterointerface. Note that the total charge of the transition must satisfy the electrical neutrality condition $Q_m + Q_d + Q_{hi} = 0$, where Q_m is the negative electron charge on the surface of the metal forming the Schottky barrier and Q_d is the positive charge provided by uncompensated donors in the semiconductor [36, 37]. Thus, the positive charge of the trapping centers of heterojunction leads to a decrease in the positive charge of the depletion region Q_d. Consequently, the width of the depletion region of the contact, its diffusion potential, and the effective height of the Schottky barrier decrease [35, 37]. A decrease in the barrier height is given by

$$\Delta\Phi_b = \frac{qN_{hi}d}{2\varepsilon},$$

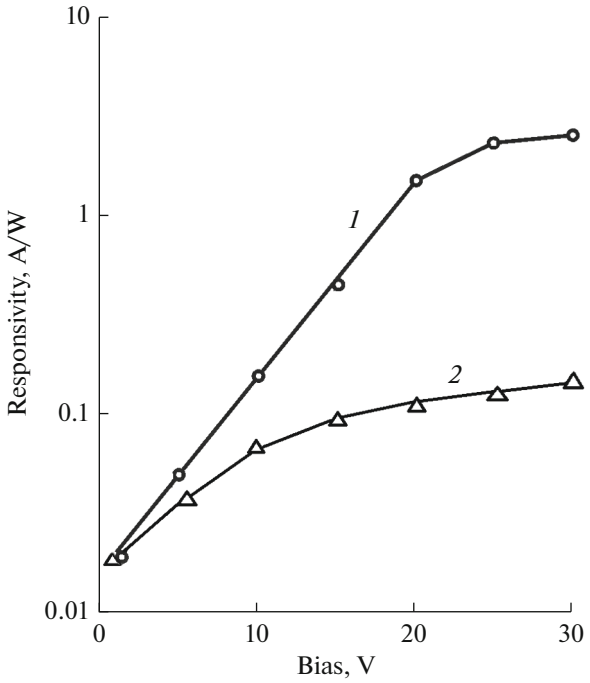

Fig. 6. Plot of the responsivity of (*1*) D2 and (*2*) D1 MSM diodes vs. bias voltage.

where N_{hi} is the density of trapping centers, d is the width of the depletion region of the reverse-biased contact, ε is the permittivity of the semiconductor, and q is the electron charge. Already at $N_{hi} = 10^{10}$cm^{-2}, a decrease in the height of the Schottky barrier under conditions for complete depletion of the intercontact region of the MSM detector is 0.25 eV, which leads to an additional component of the photocurrent of the D2 detector under irradiation in comparison with the barrier contact of the D1 diode, in which the trapping centers for carriers are missing, the barrier does not decrease, and, therefore, the photocurrent is not amplified. It is known that trapping of carriers increases with the applied bias [35]. Thus, the response signal of the D2 photodiode increases with an increase in the external bias, which leads to a quantum efficiency of the detector that exceeds the theoretical value. An accurate calculation of the photocurrent amplification of the D2 diode necessitates measurement of the distribution of the density of states (trapping centers) at the ZnCdSe/ZnSe interface and taking into account the inhomogeneous spatial distribution of the electric field in planar surface-barrier diode structures [30].

The responsivities and quantum efficiencies of the D1 and D2 detectors are in good agreement with the existing data. In particular, the ZnSe Schottky-barrier diode operates in [38] in the absence of internal amplification and, at a wavelength of 460 nm, the peak photoresponse of the detector corresponds to a responsivity of 0.1 A/W and a quantum efficiency of 27%. The

responsivity of a vertical ZnSe Schottky diode at a wavelength of 460 nm is 0.1 A/W [33]. The ZnSe MSM detector shows a responsivity of 0.128 A/W and a quantum efficiency of 36% at a wavelength of 448 nm [32], which is in good agreement with the characteristics of the D1 diode. A narrow peak of the ZnSe *p*–*i*–*n* photodiode corresponds to a responsivity of 0.17 A/W at a wavelength of 450 nm [22].

At the same time, the maximum photoresponse of the MSM diode based on interdigitated Ni contacts to ZnO at a wavelength of 385 nm corresponds to a responsivity of 1.6 A/W and the dark current is 1.04×10^{-6} A [28]. The responsivity of the MSM detector based on the (Mg,Zn)O heterostructure at a wavelength of 369 nm is 1.8 A/W [12]. A record-high responsivity for silicon detectors (1.77 A/W at a wavelength of 405 nm) has been obtained in [39] for planar metal–insulator–semiconductor–metal photodetectors fabricated on a silicon-on-insulator substrate with an *n*-type silicon active layer. Note that the aforementioned detectors exhibit quantum efficiencies that are higher than the theoretical value due to the effects of internal amplification. Thus, the results of this work are in good agreement with and, sometimes, better than the results of other authors.

CONCLUSIONS

Visible-range MSM detectors based on ZnSe and the ZnCdSe/ZnSe heterobarrier structure have been fabricated and studied, and the differences in the characteristics of the photoresponse signal and quantum efficiency of the two types of detectors have been established. The ZnSe MSM detector exhibits a broadband response in a wavelength interval of 330–465 nm with a maximum responsivity of 0.14 A/W and a quantum efficiency of 38%. Such a detector can be used in practice for detection of UV radiation that is harmful to humans. The effective narrow-band spectral response of an MSM detector based on the ZnCdSe/ZnSe/GaAs heterostructure has been experimentally determined. The peak response of the detector with FWHM = 4.3 nm and a responsivity of 2.27 A/W have been measured at a wavelength of 460 nm. Hole trapping at the ZnCdSe/ZnSe heterointerface leads to a decrease in the effective height of the Schottky barrier under irradiation of the reverse-biased junction of the MSM diode, internal amplification of the detector photocurrent, and an increase in the quantum efficiency. The narrowband response of the detector can provide efficient filtering of the desired input signal and, consequently, high noise immunity of the optical information-measurement system.

FUNDING

This work was supported by State Contract no. 0030-2019-0014.

CONFLICT OF INTERESTS

The authors declare that they have no conflict of interest.

REFERENCES

1. E. Monroy, F. Omnes, and F. Calle, Semicond. Sci. Technol. **18** (4), R33 (2003).
2. Z. Qin, D. Song, Zh. Xu, et al., Organic Electron. **76**, 105417 (2020).
3. R. A. Metzger, Comp. Semiconductors, May/June, 29 (1996).
4. T. V. Blank and Yu. A. Gol'dberg, Semicoductors **37**, 999 (2003).
5. E. Monroy, E. Munoz, F. J. Sanchez, et al., Semicond. Sci. Technol. **13** (9), 1042 (1998).
6. G. Parish, S. Keller, P. Kozodoy, et al., Appl. Phys. Lett. **75** (2), 247 (1999).
7. E. Monroy, M. Hamilton, D. Walker, et al., Appl. Phys. Lett. **74** (8), 1171 (1999).
8. Q. Chen, J. W. Yang, A. Osinsky, et al., Appl. Phys. Lett. **70** (17), 2277 (1997).
9. E. Ozbay, N. Biyikli, I. Kimukin, et al., IEEE J. Selected Topics in Quant. Electron. **10** (4), 742 (2004).
10. S. V. Averin, P. I. Kuznetsov, V. A. Zhitov, L. Yu. Zakharov, G. G. Yakushcheva, and M. D. Dmitriev, J. Commun. Technol. Electron. **50**, 367 (2005).
11. Y. Huang, D. J. Chen, H. Lu, et al., Appl. Phys. Lett. **96**, 243503-1 (2010).
12. Z. Zhang, H. Wenckstern, M. Schmidt, and M. Grundmann, Appl. Phys. Lett. **99**, 083502-1 (2011).
13. S. V. Averin, P. I. Kusnetzov, V. A. Zhitov, et al., Opt. Quantum Electron. **48**, 303 (2016).
14. H. Hong, W. A. Anderson, J. Haetty, et al., J. Appl. Phys. **84**, 2328 (1998).
15. M. Ito and M. J. Wada, Quantum Electron. **22**, 1073 (1986).
16. S. V. Averine, Y. C. Chan, and Y. L. Lam, Solid-State Electron. **45**, 441 (2001).
17. S. V. Averin, P. I. Kuznetsov, V. A. Zhitov, L. Yu. Zakharov, and V. M. Kotov, J. Commun. Technol. Electron. **50**, 202 (2005).
18. S. V. Averin, P. I. Kuznetzov, V. A. Zhitov, et al., Solid-State Electron. **114**, 135 (2015).
19. M. Sze, *Physics of Semiconductor Devices* (Wiley, New York, 1981; Mir, Moscow, 1984).
20. D. K. Schroder, *Semiconductor Material and Device Characterization* (Wiley-Interscience, New York, 1990).
21. S. Averine, Y. C. Chan, and Y. L. Lam, Appl. Phys. Lett. **77**, 274 (2000).
22. A. Bouhdada, M. Hanzaz, F. Vigue, and J. P. Faurie, Appl. Phys. Lett. **83**, 171 (2003).
23. R. Corartger, C. Girardin, J. Beauvillain, et al., J. Appl. Phys. **81**, 7870 (1999).
24. R. P. Joshi, A. N. Dharamsi, and J. McAdoo, Appl. Phys. Lett. **64**, 3611 (1994).
25. I. K. Sou, Z. H. Ma, and G. K. L. Wong, Appl. Phys. Lett. **75**, 3707 (1999).

26. A. Gerhard, J. Nurnberger, and K. Schull, J. Crystal Growt **184/185**, 1319 (1998).
27. F. Vigue, E. Tournie, J.-P. Faurie, et al., Appl. Phys. Lett. **78**, 4190 (2001).
28. N. N. Jandow, F. K. Yam, S. M. Thahab, et al., Current Appl. Phys. **10**, 1452 (2010).
29. L. Redaelli, A. Mukhtarova, S. Valdueza-Felip, et al., Appl. Phys. Lett. **105**, 131105–1 (2014).
30. S. Averin, R. Sachot, J. Hugi, et al., Appl. Phys. **80**, 1553 (1996).
31. S. Sze, D. J. Coleman, and A. Loya, Solid-State Electron. **14**, 1209 (1971).
32. T. K. Lin, S. J. Chan, Y. K. Su, et al., Mater. Sci. Eng., A **119**, 202 (2005).
33. E. Monroy, F. Vigue, F. Galle, et al., Appl. Phys. Lett. **77**, 2761 (2000).
34. A. Sciuto, F. Roccaforte, S. Di Franco, et al., Appl. Phys. Lett. **90**, 223507-1 (2007).
35. E. H. Rhoderick and R. H. Williams, *Metal-Semiconductor Contacts* (Oxford, 1988).
36. O. Katz, V. Garber, B. Meyler, et al., Appl. Phys. Lett. **79**, 1417 (2001).
37. S. Liang, H. Sheng, Y. Liu, et al., J. Crystal Growth **225**, 110 (2001).
38. F. Vigue, T. Tournie, and J. P. Faurie, Electron. Lett. **36**, 252 (2000).
39. V. Mikelashvili, Y. Shneider, A. Sherman, et al., Appl. Phys. Lett. **114**, 073504-1 (2019).

Translated by A. Chikishev